

N O T I C E

THIS DOCUMENT HAS BEEN REPRODUCED FROM  
MICROFICHE. ALTHOUGH IT IS RECOGNIZED THAT  
CERTAIN PORTIONS ARE ILLEGIBLE, IT IS BEING RELEASED  
IN THE INTEREST OF MAKING AVAILABLE AS MUCH  
INFORMATION AS POSSIBLE

(NASA-CR-164056) STRUCTURE OF THE LOW  
LATITUDE BOUNDARY LAYER (California Univ.)  
60 p HC A04/MF A01 CSCL 04A

N81-20638

Unclas  
G3/46 18943

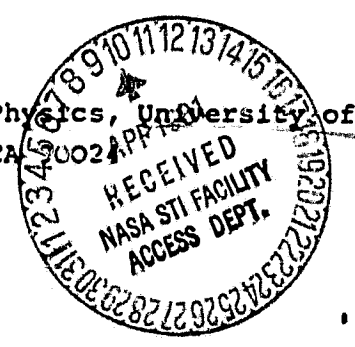
STRUCTURE OF THE LOW LATITUDE BOUNDARY LAYER

N. Sckopke, G. Paschmann, G. Haerendel  
Max-Planck-Institut für Physik und Astrophysik, Institut für  
extraterrestrische Physik, 8046 Garching, W-Germany

B.U.Ö. Sonnerup  
Dartmouth College, Hanover, New Hampshire. 03755

S.J. Bame, T.G. Forbes, E.W. Hones, Jr.  
University of California, Los Alamos Scientific Laboratory,  
Los Alamos, NM 87545

C.T. Russell  
Institute of Geophysics and Planetary Physics, University of  
California, Los Angeles, CA 90024



(Revised 1 September 1980)

## Abstract

Observations at high temporal resolution of the frontside magnetopause and plasma boundary layer, made with the LASL/MPE fast plasma analyzer onboard the ISEE-1 and -2 spacecraft, have revealed a complex quasiperiodic structure of some of the observed boundary layers: cool tailward streaming boundary-layer plasma is seen intermittently, with intervening periods of hot tenuous plasma which has properties similar to the magnetospheric population. While individual encounters with the boundary layer plasma last only a few minutes, the total observation time may extend over one hour or more. One such crossing, at 08 hours local time and  $40^\circ$  northern GSM latitude, is examined in detail, including a quantitative comparison of the boundary-layer entry and exit times of the two spacecraft. The data are found to be compatible with a boundary layer that is always attached to the magnetopause but where the layer thickness has a large-scale spatial modulation pattern which travels tailward past the spacecraft. Included are periods when the thickness is essentially zero, and others when it is of the order of one earth radius. The duration of these periods is highly variable but is typically in the range 2-5 minutes corresponding to a distance along the magnetopause of the order  $3-8R_E$ .

The observed boundary layer features include a steep density gradient at the magnetopause, with an approximately constant boundary layer plasma density amounting to about 25% of the magnetosheath density, and a second abrupt density decrease at the inner edge of the layer. It also appears that the purely magnetospheric plasma is occasionally separated from the boundary layer by a halo region in which the plasma density is somewhat higher, the temperature somewhat lower, than in the magnetosphere. A tentative model is proposed in which the variable boundary layer thickness is produced by the Kelvin-Helmholtz instability of the inner edge of the layer, and in which eddy motion provides effective mixing within the layer.

## 1. Introduction

Plasma observations performed in the outermost regions of the Earth's magnetosphere have shown the presence of a layer of magnetosheath-like plasma just inside the magnetopause. Such plasma has been found on tail field lines at low latitudes in the "magnetotail boundary layer" (Hones et al., 1972; Akasofu et al., 1973), and at high latitudes in the "plasma mantle" (Rosenbauer et al., 1975), as well as on dayside field lines at high latitudes just equatorward of the cusp in the "entry layer" (Paschmann et al., 1976; Crooker, 1977; Eastman, 1979), and at low latitudes in the "low-latitude boundary layer" (LLBL) (Eastman et al., 1976; Haerendel et al., 1978; Paschmann et al., 1978; Eastman and Hones, 1979; Eastman, 1979). It is the purpose of this paper to display and discuss certain temporal and spatial features of the LLBL, revealed by the fast plasma instrumentation onboard the satellite pair ISEE-1 and -2. A description of the ISEE spacecraft and mission may be found in Ogilvie et al. (1977).

Prior studies of the LLBL were based on two-dimensional plasma data with medium to low temporal resolution: data from the LASL plasma analyzer on IMP-6 (Eastman et al., 1976; Eastman and Hones, 1979; Eastman, 1979), and from the MPE instrument on HEOS-2 (Haerendel et al., 1978). The results reported by the two groups agree in many respects, but differ also on one important point, that concerning the predominantly observed density variation at the magnetopause and across the boundary layer. In the IMP data 50% or more of the crossings

display no distinct density change across the magnetopause, while in the HEOS observations such a change is almost always present with the density remaining at a plateau level, substantially below the magnetosheath value, throughout most of the LLBL. These different findings led the two groups to suggest different entry mechanisms: local entry, via diffusion or direct flow across the magnetopause, in the former case; nonlocal entry, e.g. in the cusps, followed by internal flow and diffusion and/or heating of cold magnetospheric plasma, in the latter. Some of the discrepancies between the two data sets are perhaps artificial and caused by the much coarser time resolution of the HEOS experiment (Eastman and Hones, 1979). There may also be a real difference, owing to the fact that the two sets do not cover the frontside magnetopause identically, with a preponderance of crossings at greater distances from the subsolar region in the IMP-6 set (Paschmann et al., 1978).

The present analysis does not suffer from a lack of temporal resolution. Like the study of Paschmann et al. (1978), it is based on data from the LASL/MPE fast plasma experiments (FPE) on ISEE-1 and -2 which in high data rate provide two-dimensional (2D) proton and electron distributions every 3 seconds, and, simultaneously, three-dimensional (3D) distributions every 12 seconds. Details of the instruments are described elsewhere (Bame et al., 1978; Paschmann et al., 1978). Here, it is sufficient to note that the 2D instruments sample protons and electrons in 16 energy bins and in 16 angular sectors of the spacecraft equatorial plane (which approximately coincides with the ecliptic plane), integrating over  $\pm 55^\circ$  of the elevation angle. By reducing the

angular resolution to 8 sectors, which is adequate for many purposes, 2D distributions can be obtained every 1.5 seconds. In addition, good approximations to the electron density and temperature can be derived from individual energy spectra; these parameters (1D data) can be analyzed with 375 milliseconds resolution, cf. Bame et al. (1979). The 3D instrument resolves the  $\pm 55^\circ$  elevation range into 4 segments, the azimuth into 8 and 4 sectors (for the inner and outer elevation channels, respectively). Its total field of view amounts (as that of the 2D instrument) to 82% of the unit sphere. Effects of the incomplete angular coverage on the accuracy of the computed plasma bulk parameters have been studied by means of simulations with Maxwellian distributions (cf. Paschmann et al., 1978). Briefly, inaccuracies grow with increasing flow elevation angles and increasing ratios of the bulk speed over the thermal speed, but even for elevations as large as  $60^\circ$  they are reasonably small as long as the temperature is above  $\sim 10^6$  K, and the bulk speed below  $\sim 300$  km/s. Ion beams can only be missed if they are highly supersonic and propagate almost perpendicular to the spacecraft spin plane. The data (cf. Figure 3) do not indicate the presence of such ions in the large part of velocity space that is sampled by the instrument. Also employed in our study are the 64 s averages of the UCLA magnetic-field data provided on the ISEE-1 data pool tape, and for certain intervals also medium resolution (12 s averages overlapping by two thirds) and high resolution (62.5 ms) field data. A description of the magnetometer experiment may be found in Russell (1978).

Sections 2-7 of the paper contain a detailed study and interpretation of a single low-latitude morning-side boundary layer crossing (November 6, 1977, orbit 7, outbound), followed in Section 8 by a brief summary of other ISEE observations of the LLBL. The November 6, 1977, pass is representative of a number of these. It was selected for several reasons, among them the high rate of data transmission, and the availability of simultaneous ISEE-1 and -2 data over most of the period of interest. But our main criterion was that one of the effects which we wish to demonstrate was less obscured by competing ones than on other occasions. This effect is the presence of a large temporal modulation of the boundary layer thickness at a fixed observation point on the magnetopause, or equivalently, a spatial modulation pattern travelling tailward past that point. In Section 9, we describe a physical model that may explain this modulation.

## 2. Overview of Observations

Figure 1 shows two hours of plasma and magnetic-field data from the ISEE-1 outbound-traversal of the outer magnetosphere and magnetosheath on November 6, 1977, starting at 0430 UT. A few brief boundary layer plasma encounters occurred in the 30 minute period preceding that time (Frank et al., 1978, Fig. 5) but the main encounter started at 0459 UT and continued intermittently for slightly more than 50 minutes, during which time the satellite travelled outward a distance of more than one earth radius. At 0550 UT it crossed the magnetopause, where the magnetic field underwent a large directional change, and entered the magnetosheath. The satellite location at that time was  $\sim 0800$  local time at  $\sim 40^\circ$  northern GSM latitude. The geocentric radial distance of the magnetopause was  $12.75 R_E$  in close agreement with the position predicted by the Fairfield (1971) model.

At the beginning of the data interval shown, the instrument sampled the hot tenuous plasma of the outer magnetosphere (region 1; identified in Figure 1 by the density level) and at the end the much denser and cooler magnetosheath plasma (region 4). These two states establish the extreme upper and lower limits on density and temperature. During the boundary layer encounter the plasma density and proton temperature switched between two intermediate states of low density and high temperature (region 2) and of higher density and lower temperature (region 3). We refer to the former region as the halo, to the latter as the boundary layer proper.

In reality there are several intermediate levels, but for the purposes of the subsequent discussion it is convenient to consider only four plasma domains, referred to as regions 1-4 above (for a geometrical model, see Figure 7). The density maxima in region 3 typically fall short of the magnetosheath (region 4) values by a factor of  $\sim 4$ , and the minima in region 2 exceed the magnetospheric (region 1) values by a factor of  $\sim 2$ . Likewise, the proton temperature minima in region 3 typically exceed the magnetosheath temperature by a factor of  $\sim 2$  while the maxima in region 2 fall short of the magnetospheric values by a factor of  $\sim 4$ . During the high density periods (region 3) the electron temperature reaches essentially the magnetosheath level, during low density ones (region 2) it falls substantially short of the magnetosphere level.

The plasma parameters shown are individual data (3 s "snapshots") spaced 24 s apart (rather than averaged over 24 s). This spacing was chosen to adjust the temporal resolution to the time interval covered; corresponding reductions apply to some of the subsequent figures. On expanded time scales, the full set of the 3 s or 1.5 s data (partially shown in later figures), and even the 1D electron data displayed every 375 milliseconds (not included) similarly show distinctly different states of the density and temperature, in the latter cases superimposed by fluctuations of the order of a factor of 2. Since we do not intend to discuss the microscale structure of the plasma, such fluctuations on time scales of less than 3 s are of no importance for our purpose; also, their influence on the 3 s data is small so that the intermediate levels shown in the figure are real and not merely artifacts created by data averaging. By using the term "level" we do not wish to imply

that the plasma density and temperature remain constant throughout such intervals. It is immediately apparent in Figure 1 that, whereas transitions from region 2 to region 3 tend to occur rapidly, the relaxation back to region 2 conditions takes place more gradually, and often step-wise. Further discussion of the plasma properties in and near the boundary layer is presented in Section 3.

Levels of plasma density and temperature intermediate between magnetosheath and magnetosphere values are among the well-known characteristics of the LLBL (Eastman et al., 1976; Haerendel et al., 1976; Eastman and Honcs, 1979), but the quasiperiodic switching between two intermediate levels, apparent in the figure, with periods in the range 2-5 min has not been reported heretofore. It is this feature that provided the main focus of the present paper.

Turning now to the plasma bulk flow panel in Figure 1, it is seen that the boundary layer plasma in the high density low temperature state (region 3) attains bulk speeds comparable to the magnetosheath value. In fact, in the density maxima immediately preceding the magnetopause it exceeds that value by approximately 50%. The velocity spikes in the magnetosheath region at 0605 UT, and perhaps also those near 0557 and 0624 UT, have the signatures of flux transfer events (Russell and Elphic, 1978). In the low-density gaps (region 2) the flow speed is, for the most part, small. More details concerning the plasma flow are given in Section 4.

The magnetic-field orientation, given by the GSM longitude and latitude angles  $\phi_B$  and  $\lambda_B$  in Figure 1, indicates that there was only one magnetopause crossing: at 0550 UT. During the preceding 50 minutes of boundary layer observations, the field orientation was magnetospheric although with a higher level of fluctuations than before  $\approx$ 0459 UT. Such fluctuations are commonly observed in the boundary layer (Eastman et al., 1976; Haerendel et al., 1978). Details of these variations are discussed in Section 5. The possibility of brief excursions into the magnetosheath which might not show up in the low-resolution field data used in the figure, can be ruled out from an inspection of the medium and high resolution data. Immediately before the magnetopause crossing the plasma was in the low-density high-temperature state (region 2), indicating that little boundary layer plasma was present. The thickness of the boundary layer at this instant, and the motion and structure of the magnetopause will be discussed in Section 6.

### 3. The Boundary Layer Plasma

The boundary layer plasma has frequently been described as being "magnetosheath-like" or a mixture of plasma from the magnetosheath and from the magnetosphere (Eastman et al., 1976; Haerendel et al., 1978; Eastman and Hones, 1979; Eastman, 1979). This description was obtained from comparisons of proton and electron spectra in the magnetosphere, magnetosheath, and boundary layer plasma, and was recently confirmed by mass spectrometer data (Shelley et al., 1978; Peterson et al., 1979). Rather than discussing individual energy spectra we present in Figure 2 the temporal variations of proton and electron fluxes in selected energy bands during the central one-hour interval of the previous figure. The parameters shown are "partial densities", i.e., the contributions from the respective energy bands to the total (2D) plasma density shown in the upper panel of Figure 1.

The upper two proton curves and the upper electron curve in Figure 2 are the low-energy parts of the spectra which dominate in the cool magnetosheath distributions. These fluxes are enhanced in the boundary layer and, since they contribute the most to the total density, lead to the density enhancements. The bottom proton and electron curves are taken from those parts of the distributions which dominate the spectra in the outer magnetosphere. These curves are invariably depressed whenever the low-energy fluxes are enhanced. In accordance with previously published results (Haerendel et al., 1978) we see that, also in this case,

the amplitude of the oscillation in the high-energy (magnetospheric) proton curve is much smaller than that of the low-energy (magnetosheath) one. The remaining two curves are from those parts of the spectra where variations are comparatively small; in particular, there are hardly any changes at the magnetopause. The maxima of the low-energy protons and electrons in the boundary layer never reach their respective magnetosheath levels, a fact reflected in the corresponding behaviour of the total density in Figure 1. Likewise do the high-energy fluxes never fall as low as in the magnetosheath.

Two more comments should be made about the curves in Figure 2. First, at the beginning of the event the transition from the magnetosphere (region 1) to the dense boundary layer (region 3) occurs, not directly, but via a brief encounter with region 2. This fact is also evident in Figure 1, in particular in the electron temperature. On the other hand, it appears that the magnetopause crossing corresponded to a more or less direct transition from region 2 to region 4 since (on this time scale) the records do not show any appreciable shoulders in the density curves to indicate a sustained presence of region 3 plasma. This point will be examined further in Section 6.

The second comment is that, at the highest as well as the lowest energies, the transitions from region 2 to region 3 are often very sharp and nearly simultaneous, while the return to region 2 is more gradual, giving the time records a saw-tooth appearance. At the intermediate energies (2.3 - 4.5 keV ions;

285 - 670 eV electrons) the 2+3 transitions are usually also rapid but the saw-tooth effect is largely absent.

The steep temporal gradients in Figures 1 and 2, associated with transitions from region 2 to region 3, do not correspond to stationary steep spatial gradients traversed at essentially the satellite speed. One indication of this may be found in Figure 2 which shows that the gradients are almost equally steep at high and low energies, contrary to what would be expected from finite gyro-radius effects in a stationary structure. In Section 7 the time delays between the ISEE-1 and 2 encounters with these gradients will be used to demonstrate that the situation is likely to have been produced by more gentle spatial gradients in density and temperature being swept by the satellite with speeds comparable to the plasma flow speed in the boundary layer.

In summary, the energy composition of the plasma in region 3 is consistent with the view that the boundary layer contains a mixture of the magnetosheath and magnetospheric components. In the discussion section we shall present a possible qualitative model which accounts for the formation of both regions 2 and 3 via a combination of eddy and microscopic diffusion processes.

We turn now to a brief discussion of the interrelationship of density and temperature variations during the 50 minute boundary layer encounter. The top two panels in Figure 3 show that the density and temperature curves are almost perfect mirror images

of each other, the implication being that the product of  $N$  and  $T$ , i.e., essentially the pressure, varies much less than  $N$  and  $T$  individually. This latter effect is shown by the plasma pressure (lower curve) in the third panel. The remaining variations in  $p$  are such that the pressure tends to be low when the plasma density is high. These pressure fluctuations are balanced to a considerable extent by the magnetic pressure  $B^2/8\pi$  which is slightly higher in the high density regions so that the total pressure ( $p + B^2/8\pi$ ), shown as the upper curve in the third panel of Figure 3, remains nearly constant. An exception is the large and unexplained pulse in magnetic (and total) pressure near 0548 UT.

#### 4. Plasma Flow Properties

To study the plasma flow behaviour in detail, we employ the three-dimensional FPE data. As a compromise between the conflicting demands of high time and high angular resolution we show, in panels 4-6 of Figure 3, 24 second sliding averages of the 3D flow vectors as well as the 2D (3 second) data of the bulk speed. The latter information can be used to identify rapid variations which may lead to time aliasing of the 3D data.

The flow direction is given by the angles  $\alpha_D$  and  $\epsilon_D$  which are measured in a co-ordinate system associated with the boundary normal. This right-handed cartesian system (NOR) is defined as follows: the  $z_N$  axis is parallel to the outward-directed normal, to the magnetopause, while the  $x_N$  axis lies in the plane defined by the Earth-Sun line and the  $z_N$  axis, and points towards the tail. The angles  $\alpha_p$  and  $\epsilon_p$  measure the azimuth in the tangential  $(x_N, y_N)$  plane and the elevation from this plane, respectively, with  $\epsilon_p > 0$  indicating an outward directed flow component. The normal vector employed in the diagrams was the Fairfield (1971) model normal. It has solar ecliptic (GSE) cartesian coordinates (0.674, -0.682, 0.283) and coincides rather closely with the minimum-variance normal calculated from the magnetic field vectors in the magnetopause (see Section 6).

The NOR system was chosen to facilitate a comparison of the boundary layer flow with the external (magnetosheath) flow: Just outside the magnetopause, a perfectly axisymmetric flow

around the magnetosphere would be characterized by  $\alpha_p = \epsilon_p = 0$ . Consequently, when  $\alpha_p = \epsilon_p = 0$  in the boundary layer, the plasma flows approximately parallel to the exterior plasma. Contrary to expectations, both  $\alpha_p$  and  $\epsilon_p$  deviate from zero after 0550 UT, and both angles show certain quasi-periodic variations. These oscillations are caused by an instrumental effect: since the magnetosheath plasma was rather cool on this occasion, the ion distributions were not adequately resolved by the 3D instrument. The same effect is also responsible for the noticeable differences between the 2D- and 3D bulk speed curves in this interval (panel 4). At least part of the deviation of the average computed flow direction from the expected direction (in the observed sense) results from the instrument's systematic underestimate of the flow component parallel to the spacecraft spin axis which is no longer negligible under the present circumstances. Another plausible reason for this deviation is that the magnetopause orientation may have changed in association with the inward motion at 0550 UT, cf. Section 6. (Note, however, that in a NOR system based on the minimum variance normal rather than on the model one,  $\epsilon_p$  is even more negative.) Nevertheless, the mean deviations of the computed magnetosheath flow angles from zero are sufficiently small to permit the use of  $\alpha_p = \epsilon_p = 0$  as the reference for the boundary layer flow directions.

The bulk flow speed generally starts to increase nearly coincident with, but sometimes slightly preceding, the rapid density increases at the region 2  $\rightarrow$  3 transitions. This initial velocity increase is considerably less rapid than the density increase, while the velocity decrease is more rapid than the density decrease during the return from region 3 to region 2. Thus the

bulk speed pulses do not have the saw-tooth shape of the density (and temperature) pulses.

The flow angles  $\alpha_p$  and  $\epsilon_p$ , shown in Figure 3 only for particle fluxes exceeding  $10^7 \text{ cm}^{-2} \text{ s}^{-1}$ , also display a characteristic behaviour during the flow pulses. In most cases the azimuth angle  $\alpha_p$  remains near zero while the elevation angle  $\epsilon_p$  changes from negative in the early part to positive in the late part of the pulse. This result indicates the presence of a substantial flow component inward from the magnetopause during the early part, outward during the late part, of the flow pulse. Near the pulse maxima the flow is usually approximately parallel to the magnetosheath flow. Hence, most of the boundary layer plasma is flowing approximately parallel to the external flow. When the bulk speed is low, on the other hand, the direction is generally more variable (partly for instrumental reasons), but sometimes there are short intervals (e.g., 0503 - 0506 UT) when the boundary layer plasma has a flow component that is nearly anti-parallel to the magnetosheath flow. Some of the above flow characteristics could in theory be the result of a  $\underline{B} \times \underline{v}_p$  drift but no consistent relationship between  $\underline{v}_p$  and  $\epsilon_p$  has been found. Thus we conclude that the observed inward-outward flows are associated with radial  $\underline{E} \times \underline{B}$  motion of the boundary layer plasma. Studies of these effects using time delays between the two satellites are presented in Section 7.

### 5. Magnetic Field Observations

The magnetic field vector is shown in the three bottom panels of Figure 3, with the field orientation given by an azimuth angle  $\alpha'_B$  and an elevation angle  $\epsilon'_B$ . These angles are measured in the right-handed cartesian LMN coordinate system associated with the local magnetopause normal as described by Russell and Elphic (1978). Again the  $z'$  axis (N) is along the outward (model) normal, but the  $x'$  axis (L) is due north and is such that the GSM  $z$  axis lies in the  $(x', z')$ , or  $(L, N)$  plane. The azimuth angle  $\alpha'_B$  lies in the LM plane and is measured from the L (or  $x'$ ) axis. The NOR and LMN systems differ only by a rotation around the common  $z = z'$  axis, i.e. in the azimuth angle; in the present case,  $\alpha = \alpha' - 60^\circ$ , cf. the NOR scale given on the right-hand side of the  $\alpha'_B$  panel. Thus, when  $\alpha_p = 0$  and  $\alpha'_B = 0$ , (and  $\epsilon_p = \epsilon'_B = 0$ ), the angle between flow and field is  $\approx 60^\circ$ . Also, positive excursions of  $\alpha'_B$  from zero imply that the tangential field component is rotated tailward, towards the plasma flow direction.

In the magnetosphere  $\alpha'_B$  is approximately zero while, contrary to expectations,  $\epsilon'_B$  has a substantial negative value. Since the LMN  $x'$  axis (L) was not parallel to the dipole meridional plane at this time, but was tilted sunward with respect to that plane, the former result indicates that the magnetic field lines were swept back towards the tail in accordance with standard models of the geomagnetic field (cf. Mead and Fairfield, 1975; Figure 5). The negative  $\epsilon'_B$  angle in regions 1 and 2 is more puzzling. It could again indicate that the orientation of the magnetopause normal during the boundary layer encounter period

was different from that of the model normal. This interpretation is supported by the fact that, after the magnetopause crossing at 0550 UT,  $\alpha'_B$  was close to zero (the magnetosheath  $\alpha'_B$  value is off-scale in Figure 3 but is  $-170^\circ$  initially, cf. Figure 5). Assuming that the magnetopause orientation was stable over a sufficiently long interval, and that the boundary was a tangential discontinuity, we can enforce  $\alpha'_B = 0$  on both sides by taking the cross product of an inner and outer field vector for the normal direction. Choosing vectors near 0529 and 0554 UT when the field was relatively quiet, we obtain a normal with GSE components (0.550, -0.674, 0.494). Its z component is significantly larger than that of the model normal (0.674, -0.682, 0.283) and is difficult to reconcile with the given spacecraft location. Another possibility is that the satellite pair remained at a rather large distance from the magnetopause during most of the boundary layer encounters. At high latitudes near the southward edge of the cusp the magnetic field develops a substantial inward component even at relatively modest distances from the magnetopause. It will be shown in the next section that the magnetopause at the time it was penetrated moved inward at a rate of  $\sim 50$  km/s. At this speed, a distance of  $1 R_E$  is traversed in only 2 minutes.

The magnetic field undergoes systematic changes during the transitions back and forth between regions 2 and 3. During the rapid density increases in the 2 + 3 transitions  $\alpha'_B$  and  $\alpha'_B$  both increase. The former change corresponds to a field aligned current flowing toward the equator, the latter to a

tipping of the field vector to a position more parallel to the magnetopause. In addition, the field magnitude is slightly enhanced, indicating an increase of the field tension in association with the positive excursions of the angles. These variations will be discussed at the end of Section 9. After 0543 UT these systematic features cease. For example, during the large field magnitude pulse near 0548 UT,  $\alpha'_B$  is negative.

## 6. Magnetopause

The orientation and magnetic structure of the magnetopause current layer has been examined by use of the minimum variance analysis (for a review, see Sonnerup, 1976). The resulting normal vector, obtained from the ISEE-2 data set, has the GSE components (0.693, -0.713, 0.102) with an estimated uncertainty in orientation of only  $\pm 5^\circ$ ; the results from ISEE-1 are essentially the same. This normal differs by an angle of  $10^\circ$  from that of the Fairfield (1971) model which has the GSE components (0.674, -0.682, 0.283). The latter was used for the data presentation in Figure 3 because the distortion indicated by the small GSE z component of the minimum-variance normal vector may not have persisted throughout the boundary layer encounter.

The structure of the magnetopause is shown in Figure 4 which contains, on the left, a polar plot of the tangential field components,  $B_i$ , and  $B_j$ , along the maximum and intermediate variance directions, respectively, and on the right, the normal field component,  $B_k$ , versus  $B_i$ . It is seen that the tangential field undergoes a well ordered rotation from its magnetospheric ( $B_i > 0$ ) to its magnetosheath ( $B_i < 0$ ) direction. The rotation angle is nearly  $180^\circ$ . The normal field component has an average value of  $0.3 \pm 0.7$  nT and is therefore not significantly different from zero.

P Since the plasma bulk flow speed exceeds the magnetosheath speed by a considerable amount in three of the boundary layer plasma encounters preceding the magnetopause crossing (see Figure-3), it is of interest to ask whether these high speeds could have been caused by local magnetic field reconnection as in the case described by Paschmann et al. (1979). The reconnection model requires the tangential velocity change  $\Delta \underline{v}_t$  and magnetic field change  $\Delta \underline{B}_t$  across the magnetopause to be colinear. However, such is not the case. The high plasma velocities in the boundary layer are approximately parallel to the magnetosheath flow vectors, i.e.,  $\Delta \underline{v}_t$  is tailward (along NOR-x), while  $\Delta \underline{B}_t$  is along the maximum variance direction, which is almost parallel to the LMN-L direction. Hence the two vectors are mis-aligned by about  $60^\circ$ . Furthermore, the velocity change predicted by the reconnection model,  $|\Delta \underline{B}_t| / (\mu_0 \rho)^{1/2}$ , is about 200 km/s while the observed  $|\Delta \underline{v}_t|$  is less than 100 km/s. This disagreement between the measured local  $\Delta \underline{v}_t$  and the one predicted by theory does not exclude the possibility that the boundary layer plasma was accelerated by reconnection as it crossed the magnetopause somewhere upstream of the observation point. However, an entirely different explanation for the observed boundary layer velocity peaks is also possible and will be presented in the discussion section.

It is also of interest to establish the thickness and speed of the magnetopause as well as the thickness of the layer just inside the magnetopause in which the plasma density decreases down to the region 2 level. This can be done with the aid of

Figure 5 which shows plasma density and field angle  $\alpha'_B$  for both ISEE-1 and -2 as a function of time. It is seen that the outer satellite, ISEE-1, encountered the magnetopause approximately 10 s earlier than the inner one. Since the component of the satellite separation vector along the minimum variance normal was  $\sim 500$  km one concludes that the magnetopause moved inward with a speed of approximately 50 km/s at the time of the crossing. The duration of the magnetopause current layer is about 20 s so that its thickness was of the order of 1000 km. For ISEE-2, the density increase from the region 2 level to the magnetosheath one commences approximately 4 s prior to the inner edge of the magnetopause and is essentially complete at the latter location. Thus at this time the density ramp, i.e., the boundary layer, had a thickness of only about 200 km. For ISEE-1, the magnetic field rotation started at about the same time as, or even slightly prior to the density increase, indicating that no boundary layer was present. The different slopes and other features of the ISEE-1 and -2 curves during the crossing indicate that substantial changes in magnetopause velocity and/or in plasma and magnetic structure occur on time scales of the order of 10 s.

## 7. Interpretation

In order to develop a conceptual model which orders the observations discussed in the previous sections, it is necessary first to examine the time delays between the ISEE-1 and -2 encounters with the boundary layer (region 3) plasma. This is done in Figure 6, which shows the ISEE-1 and -2 ion densities, as a solid curve and as dots, respectively, during the major part of the boundary layer encounter; the remaining period, that immediately preceding the magnetopause crossing, may be found in Figure 5. In examining these figures it is important to remember that ISEE-1 was 500-550 km closer to the magnetopause than ISEE-2, and that the separation vector between the two satellites formed only a small angle with the nominal magnetopause normal.

The most striking feature in Figure 6 is that, for the most part, ISEE-1 entered the boundary layer (region 3) before, and left that region after, ISEE-2. There is no single instance where ISEE-2 entered region 3 before ISEE-1 as would occur if the boundary layer consisted of plasma sheets (or blobs) separated from the magnetopause, and the satellites were traversing a sheet surface facing the magnetopause. There are a few isolated instances when an exit from region 3 was nearly simultaneous for the two satellites and even when ISEE-1 exited somewhat before ISEE-2. But the preponderance of the timing evidence in Figure 6, including several instances when region 3 plasma was seen by ISEE-1 and not by ISEE-2 (e.g. near 0505 and 0513 UT),

indicates that the satellite pair crossed into and out of region 3 across an interface located on the earthward side of that region. In other words, there is no evidence in the present data set that requires a detached boundary layer. Below, we discuss three models, all of which have an attached boundary layer, and all of which are consistent with the basic observation that the boundary layer (region 3) plasma was seen intermittently during the 50 minute period preceding the magnetopause crossing and, in particular, that it was essentially absent adjacent to the magnetopause crossing. These models are also shown in Figure 7.

Model A consists of a plasma layer attached to a smooth magnetopause surface. The plasma moves tailwards and the layer thickness is essentially independent of the tailward coordinate  $x_N$ . The magnetopause and boundary layer together execute a quasi-periodic inward/outward motion. In addition the boundary layer thickness varies with time in such a manner that it happens to be nearly zero at the time of the magnetopause encounter.

Model B is similar to model A except that the inward/outward motion of the system is replaced by an undulation of both magnetopause and boundary layer to form a tailward moving wave train.

Model C has a smooth and generally nearly stationary magnetopause surface with an attached plasma layer, the thickness of which is a function of  $x_N$ . This layer moves tailward with the

result that a satellite crossing the region will observe the boundary layer plasma intermittently. The modulation of the boundary layer (region 3) thickness is large and incorporates values near zero. Thus the model can be described as field-aligned plasma blobs sliding along the magnetopause. The radial width of these blobs is of the order of one earth radius. Their length in the flow direction is typically  $3-8 R_E$ , based on a duration of 2-5 minutes and a flow-speed of 150 km/s. The individual blobs are sometimes connected via narrow necks along the magnetopause but are sometimes entirely disconnected. The leading and trailing edges may be steep, as shown in the figure. On the basis of the behaviour of shear layers in ordinary hydrodynamics it may also be presumed that the blobs contain substantial vortex motion in the sense indicated in the figure. As discussed in Section 6, inward motion of the entire magnetopause-boundary layer system with  $\sim 50$  km/s must have occurred during the magnetopause encounter.

In discussing the advantages and disadvantages of the three models it is first noted that each incorporates certain ad hoc elements. In all models it must be assumed that the boundary layer (region 3) thickness happened to be nearly zero at the time of the magnetopause crossing. Model C has the advantage that it implies the regular occurrence of a vanishing or nearly vanishing thickness. On the other hand, in model C it is necessary to assume the onset of inward motion of the magnetopause and boundary layer at the time of the crossing of that layer. Such motion is a regular part of models A and B.

During the 50 minutes prior to the magnetopause crossings, all three models may require a slow outward motion of the magneto-

pause and boundary layer with the satellite pair in order to account for the fact that they all predict, but the data set does not show, a systematically increasing time duration of the region 3 encounters and a decreasing duration of the intervening gaps (region 2) as the satellite pair progresses outward. Such slow magnetopause motion has been reported (Aubry et al., 1970) but in the context of the present models it represents an ad hoc additional assumption. In model C steep leading and trailing edges of the plasma blobs may in part eliminate this difficulty.

Turning now to the more definite predictions of each model, it is first seen that models A and B predict a high likelihood of multiple magnetopause crossings whereas model C does not. Since only a single crossing was observed, model C has a definite advantage. Models A and C both predict inward plasma motion during the early part, outward motion during the late part, of an encounter with region 3, while model B has the opposite prediction. Furthermore, model B, but not models A or C, predicts a sunward tilt of the magnetopause normal vector at the time of the magnetopause crossing. The data do not indicate a significant tilt in that direction, as can be judged from the smallness of the angle between the minimum variance and model normal vectors mentioned in Section 6. Model C, but not models A and B, may account for the occasional occurrence of situations where ISEE-2 leaves region 3 before ISEE-1. This situation requires a negative slope of at least part of the trailing edge of a plasma blob as shown in Figure 7. Such a situation would not occur in model B unless the magnetopause develops severe folding.

P

On the basis of these results it appears that, among the three models, C offers the best explanation of the observed plasma data. However, it is also evident that some elements of at least model A and perhaps also model B may have been present. In other words, we do not argue that the magnetopause has no radial motion and no small-amplitude, long-wave length waves. We do argue that the dominant contribution to the quasiperiodic entry into, and exit out of, the boundary layer (region 3) is likely to have been produced by plasma blobs sliding tailward along the magnetopause, as assumed in model C.

In order to check the validity of model C further and learn more about the shape of the plasma blobs we have used the time delays between the two spacecraft for region 2' → 3 and 3 → 2 crossings to calculate the vector normal  $\underline{n}$  to the interface between the two regions. Denoting the time delay ( $t_2 - t_1$ ), and the separation vector ( $\underline{r}_2 - \underline{r}_1$ ), between ISEE-2 and -1 by  $\Delta t$  and  $\Delta \underline{r}$ , respectively, we have

$$(\underline{V} \Delta t - \Delta \underline{r}) \cdot \underline{n} = 0$$

This relation is based on the assumption that  $\underline{n}$  and  $\underline{V} \cdot \underline{n}$  remain unchanged during the interval  $\Delta t$ . If one further assumes the interface to be field aligned so that

$$\underline{B} \cdot \underline{n} = 0$$

it follows that

$$\underline{n} = \pm (\underline{U} \times \underline{B}) / |\underline{U} \times \underline{B}|$$

where

$$\underline{U} \equiv (\underline{V} \Delta t - \Delta \underline{E}).$$

In order to remove the ambiguity of the sign of  $\underline{n}$  we require that  $\underline{V} \cdot \underline{n} > 0$  for positive density gradients (leading edges), and  $\underline{V} \cdot \underline{n} < 0$  for the negative ones (trailing edges). The resulting normal vectors will point from the boundary layer into the halo,

Another expression for the interface normal can be obtained by computing the cross product,  $\underline{B}_2 \times \underline{B}_3$ , of field vectors taken from either side of the boundary. This method is also based on the assumption that the interface is field aligned (i.e., a tangential discontinuity) but it is independent of the plasma measurements. It fails, of course, when the field rotation is small.

The results of both methods are shown in Figure 8 as projections of boundary layer normals onto the  $(x_N, z_N)$  plane of the NOR system in which  $z_N$  is the model magnetopause normal, and  $x_N$  is the direction of the axisymmetric (tailward) magnetosheath flow. Letters (a)-(l) refer to the respective density gradients in Figure 6. The time delays  $\Delta t$  were determined from the 1D electron data (not shown). Sectors with radii of short and intermediate length indicate the range of normal directions obtained from the  $\underline{U} \times \underline{B}$  method, using data on the low and on the high density side of the discontinuity, respectively. The spread in angle is associated with uncertainties in  $\Delta t$  and fluctuations in  $\underline{B}$ . Because of the comparatively

long cycle time (12 s) of the 3D instrument, only one plasma data point from either side of the gradient was employed. Uncertainties due to statistical errors of the plasma bulk speed are not displayed. They are likely to be of the same order as those shown, particularly for the data from the halo region where  $V$  is usually small. The long arrows result from the  $\underline{B}_2 \times \underline{B}_3$  method. They represent the averages over up to 9 values. Arrows were not drawn when the field rotation was less than  $15^\circ$  for all individual vector pairs. In this context, it is significant to note that such normal vectors could not be reliably determined for several of the diagrams on the right. The explanation is found in Figure 3 which shows that across trailing plasma edges the field rotation is generally smaller (and more gradual) than across the leading edges.

In some of the examples the three normal directions differ quite significantly from each other. This, as well as the occasionally large spread in angle of an individual normal, indicates that variations of the plasma and field parameters occurred in less than 9 s or 12 s which are the sampling and averaging intervals for the (3D-) plasma and (medium resolution) field data, respectively. (Although uncertainties of the plasma data were not taken into account explicitly they are implicitly present nevertheless: a close look at Figure 6 shows that some of the density gradients have different slopes in the ISEE-1 and -2 data, indicating a change in bulk speed within a few seconds. In such cases, the underlying assumption that  $\underline{V} \cdot \underline{n}$  is identical

on the two sides of the discontinuity breaks down. In view of all these uncertainties we consider the agreement between the normals within each of the double columns in Figure 8 as remarkably good. Deviations of the directions from those expected for leading and trailing edges (e.g., example c) will be discussed below.

The first noteworthy feature in Figure 8 is that, with the exception of one case (event k, ISEE-1), all of the  $\underline{U} \times \underline{B}$  normals have negative  $z_N$  components. In other words, the vectors point towards the magnetosphere. Since the normals were chosen to point from the boundary layer into the halo this result implies that none of the crossings had the signature of a boundary layer detached (and separated by halo or magnetospheric plasma) from the magnetopause.

The second remark concerns the  $x_N$  components of the normals. Almost all cases suggest that the inner boundary of the boundary layer was tilted relative to the model magnetopause. Furthermore,  $\underline{n} \cdot \underline{x}_N$  is positive for the majority of the leading edges, and negative for the trailing edges. Since we have applied the constraint  $\underline{v} \cdot \underline{n} \geq 0$  for leading and trailing edges, respectively, this is what would be expected for models C and B in Figure 7 if the boundary layer flow always had a component parallel to the exterior flow ( $\underline{v} \cdot \underline{x}_N > 0$ ). However, as already pointed out in Section 4, the boundary layer plasma occasionally has a sunward flow component. It is for such periods that the  $x_N$  components of the normals in Figure 8 have the apparently wrong sign. In particular, in case c the plasma flows towards the sun during the entire period although partly at rather low flux levels so that the flow variables are not continuously displayed in Figure 3.

P

The relative orientation in Figure 8 of the normal vectors at entry into and exit from the boundary layer blobs indicates that the slope of the boundary layer edge relative to the magnetopause is frequently steeper at the trailing (exit) than at the leading (entry) edges. A straightforward interpretation of the saw-tooth structure of the boundary layer encounters in Figure 3 would indicate the opposite behavior: the rapid entries should correspond to steep slopes and the gradual exits to gentle ones. A plausible explanation for this apparent inconsistency in the observations is that the trailing edges are ragged and that the selection of events for the time-delay analysis underlying Figure 8 is strongly biased toward the steepest slopes.

### 8. Other Observations

So far, our discussion has concerned only a single case. We now briefly discuss some of the other observations. During their first year of operation, ISEE-1 and -2 provided data from over 120 passes across the outer magnetosphere and magnetopause between 0400 and 2000 hours local time, and between +40 and -20° GSM latitude. This number is too large to permit examination in as much detail as the crossing discussed above but we have surveyed low resolution (1 minute) data from most of the passes, and full-resolution data from many of them.

Some 20 of the flank orbits showed the presence of the plasma mantle, for example, the plasma was streaming tailward along the magnetic field. In the other cases, the boundary layer flow had a significant cross-field component which is typical for the low-latitude layer. The appearance of the boundary layer spanned the entire range found in the surveys of Haerendel et al. (1978), and Eastman and Hones (1979), from virtually no boundary layer plasma to layers of intermediate and comparatively long duration, some of them with only one crossing of the magnetopause, others with multiple crossings. It is worth pointing out that it was difficult to find even a few crossings in which the boundary layer density decreases smoothly with time from the magnetosheath density towards the magnetospheric value. Instead, many of the passes contained the main feature of the example studied here: the recurrent appearance of boundary layer plasma, at inter-

mediate density levels, alternating with magnetospheric-like plasma. Usually, the total duration was comparatively short (20 minutes or less), and often, several magnetopause crossings occurred.

There were three crossings (outbound orbits 12, 26, and 28) with complete data coverage for which the data looked very similar to Figure 1: all showed the intermittent presence of boundary layer plasma for 50 minutes or more, followed by a single magnetopause crossing. Unfortunately, the rate of data transmission was low in all three cases, i.e., 4 times lower than for orbit 7, so that precise timing studies could not be performed. One of these crossings, shown in Figure 9, occurred near the location of the November 6, 1977, crossing; the other two were located at low latitudes near the dawn meridian. There are two differences between Figures 1 and 9. First, the density and temperature in the latter case tended to return to their magnetospheric levels in the gaps between the intermittent boundary layer encounters. Thus the region 2 plasma was essentially absent. Second, in Figure 9 but not in Figure 1 boundary layer plasma (at densities up to the magnetosheath level) was present for a substantial time interval just prior to the magnetopause crossing near 0632 UT. Neither feature is in conflict with model C. In all other aspects the two crossings are remarkably similar, including the sense of the magnetic-field variations during the boundary layer encounters (a rotation towards a more tailward and outward pointing direction concurrent with an increase of the field magnitude), as can be seen in some cases even in the low-resolution data of Figure 9.

P It is interesting to compare the detailed observations obtained with the ISEE instruments with the results of the HEOS-2 survey by Haerendel et al. (1978). For orbit 7 outbound, we have simulated the long sampling interval (~ 86 s) and even longer repetition cycle (256 s) of the HEOS instrument by adding up an appropriate number of ISEE distributions. The resulting time plot (not shown) looks strikingly similar to Figure 11a of Haerendel et al. which qualified in their study as a thick layer ( $> 0.5 R_E$ ) with low density ( $n < 0.25 n_{MS}$ ). In the overviews shown in their Figures 1 and 3, such crossings were represented by large encircled crosses. It is worth pointing out that in this simulated data set the boundary layer density tends to form a plateau a factor of 2-3 below level 3 of Figure 1. This tendency was in fact conjectured by Eastman and Hones (1979), and finds its explanation in the observation that the apparent period of the density variations is comparable to that of the sampling pattern of the HEOS-2 instrument. Nevertheless, a density jump between regions 3 and 4 (albeit of a smaller magnitude than that deduced by Haerendel et al. (1978) from HEOS-2 data) seems to be a frequent feature of the frontside low-latitude boundary layer.

### 9. Discussion

In the previous section we have established that model C explains the observations in considerable detail. The model has, however, been presented entirely in geometrical terms. It is now desirable to examine whether support for it may be found in terms of physical processes.

We first ask whether the boundary layer could have been populated by diffusion across the magnetopause. Assuming an average plasma boundary layer thickness, density, and flow speed, of  $1/2 R_E$ ,  $8 \text{ cm}^{-3}$ , and  $150 \text{ km/s}$ , respectively, we obtain a total boundary layer particle flux per unit height of  $3.8 \cdot 10^{18} \text{ m}^{-1} \text{ s}^{-1}$  at the spacecraft location. With a flow distance from the subsolar point of  $18 R_E$  the magnetopause area across which this flux must enter is approximately  $5.7 \cdot 10^7 \text{ m}^2$ . Thus the average diffusive particle flux across the magnetopause is  $6.7 \cdot 10^{10} \text{ m}^{-2} \text{ s}^{-1}$ . This flux should approximately equal  $D \Delta n / h$  where  $D$  is the diffusion coefficient,  $\Delta n$  the density change across a diffusion layer of thickness  $h$ . Using the value  $D = 10^9 \text{ m}^2/\text{s}$  as an example, and a magnetosheath density of  $35 \text{ cm}^{-3}$ , we have  $\Delta n = 35 - 8 = 27 \text{ cm}^{-3}$ . Thus the thickness  $h$  can be calculated and is found to be  $\sim 400 \text{ km}$ . This is of the order of the measured magnetopause thickness and we conclude that the observations are compatible with the hypothesis that the boundary layer was formed by diffusion across the magnetopause with an effective diffusion coefficient  $D$  of  $10^9 \text{ m}^2/\text{s}$ . If, however, the real value for  $D$  is substantially less, some other entry

process must be operative upstream of the observation point. The flux-transfer like variations outside the magnetopause may have a bearing on this possibility. Clearly, our analysis does not provide an unambiguous answer to the question of the plasma entry mechanism.

Substantial diffusion across the magnetopause occurs only in the presence of a very steep density gradient there. In our estimate above, the density decreased from 35 to 8  $\text{cm}^{-3}$  in a distance of only 400 km. Large gradients are indeed frequently seen. In the November 6, 1977, case the situation was extreme at the time of the magnetopause crossing because virtually no boundary layer plasma was present adjacent to the magnetopause and the density dropped from 35 to 1  $\text{cm}^{-3}$  in a distance of only 200 km (see Section 6). One must presume that the distance scale is similar during passage of the boundary layer blobs. Note that we also expect, and do indeed observe, a steep gradient in the density of outward diffusing magnetospheric particles at the magnetopause (Figure 2).

We next ask how it is possible, in a diffusion model, to have a steep density gradient at the magnetopause followed by a more or less constant density across a boundary layer as thick as perhaps  $1/2 R_E$ , on the average, with another steep density decrease at the inner edge of that layer. It seems likely to us that such a situation will arise because of eddy transport in the boundary layer. Such transport was originally suggested by Haerendel (1978) to operate mainly in the entry layer where

it could be driven by pressure fluctuations associated with hydrodynamic turbulence of the exterior cusp flow. It is also known to develop spontaneously and to be exceedingly efficient in ordinary hydrodynamic shear layers. We see no reason why it should not be operative in the low-latitude boundary layer too, moving high as well as low energy particles. As already mentioned, this feature has been incorporated in model C and it is supported by the measured plasma flow in the blobs. The eddy motion is expected to be two-dimensional and field aligned, involving the interchange motion of flux tubes. This interchange motion is likely to be impeded to some extent by the ionosphere. However, this impediment may be rather minor in the fast moving boundary layer. The reason is (e.g. Sonnerup, 1980) that this layer must decouple itself relatively efficiently from the ionosphere, by means of field-aligned potential drops, in order to avoid excessive ionospheric electric fields and field-aligned currents. At the inner edge of the boundary layer this decoupling ceases. There the plasma velocity drops rapidly and further inward transport of plasma originating in the magnetosheath, as well as outward transport of magnetospheric particles, can no longer be achieved via eddy motion. It must again occur principally via the more inefficient microscopic diffusion. For this reason, steep outward gradients in the high-energy ones, are expected, and are also seen (Figure 2), at the inner edge of the boundary layer (region 3).

The boundary layer halo (region 2) may also have been formed by inward diffusion of boundary layer plasma. Even though this transport process is inefficient it may lead to a relatively thick halo. For example, if we assume a tailward flow speed  $V_0 = 25 \text{ km/s}$  in the halo, the diffusive thickness at the observation point is of the order of  $(DL/V_0)^{1/2}$ , where  $L$  is the flow length from the subsolar point ( $L = 18 R_E$ ). Again using  $D = 10^9 \text{ m}^2/\text{s}$  we find the thickness of the halo to be - 2000 km. We cannot exclude the possibility that some process in addition to microscopic diffusion is operative in the halo. In particular, some eddy motion may be expected in the wake of each plasma blob in model C.

We turn now to a discussion of the mechanism leading to the formation of plasma blobs. One prominent possibility is that the upstream source of the boundary layer plasma, whether it be entry at specific locations, reconnection patches, or regions of efficient diffusion, is switched off and on periodically. Since the entry process is unknown we are not in a position to examine how its efficiency could be modulated to form the observed blobs. However, there exists an entirely different explanation for the formation of the blobs. It may be argued (Sonnerup, 1980) that a boundary layer of constant thickness should be expected to break up into blobs as a result of the Kelvin-Helmholtz instability operating, not at the magnetopause, but at the inner edge of the boundary layer. The

principal stabilizing effect is provided by the magnetic-field shear, created by field-aligned currents. This shear is relatively small at the inner edge of the boundary layer (Figure 3), while in the magnetopause itself it is large (Figure 4). Further, the principal destabilizing effect, the velocity gradient, is substantial at the former location (Figure 3) but probably only modest at the latter (Figure 3). Coupling to the ionosphere is expected to impede, but not prevent, the interchange motions required for growth of the instability. The question needs to be examined whether the growth rate of the instability is sufficiently large to allow development of blobs in the time it takes the boundary layer plasma to travel from the subsolar point (as the most distant possible region of entry) to the region of observation.

The development of the Kelvin-Helmholtz instability at the interface between regions 3 and 2 might be expected to lead to a thinning of the halo (region 2) over the wave crests and a filling in of the valleys between the crests, as shown in Figure 7. By following the satellite path relative to the moving plasma in that figure, it then becomes clear why the ISEE satellites observed only a brief passage through region 2 just prior to the first boundary layer encounter at 0459 UT and why they never again sampled purely magnetospheric plasma but only region 2 and 3 plasma during the subsequent 50 minutes.

In a more speculative vein, we observe that if the Kelvin-Helmholtz waves travel at a speed somewhat less than the average plasma speed in the boundary layer, then, in the frame of the waves, the plasma still has a net tailward flow component. Mass conservation then suggests increased tailward flow speeds in the narrow necks, adjacent to the magnetopause, which connect the plasma blobs. This may provide a plausible explanation for the high boundary-layer velocities observed prior to the magnetopause crossing (Figures 1 and 3). However, the alternate possibility, that these velocities are associated with reconnection somewhere upstream of the satellite, cannot be excluded.

A final comment concerns the direction of the field-aligned currents observed at the interface between regions 2 and 3. As already mentioned, these currents flow toward the equator and perhaps the southern auroral ionosphere, rather than into the northern one. Thus they are opposite to the currents predicted by Eastman et al. (1976) as the result of distributed momentum transfer from the magnetosheath and boundary layer plasma flow to the polar-cap ionosphere via the terrestrial magnetic field. These authors suggested that such transfer is taking place over the entire front side of the magnetosphere. In an earlier paper, Haerendel and Paschmann (1975) had developed a similar dynamo model, but they suggested that the transfer is more or less confined to the entry layer, i.e. to high latitudes. Both models have in common that poleward of the transfer site the currents (on the dawn side) are flowing into the nearby ionosphere. But with a localized source as in the latter one, some

fraction of the current could also flow towards the equator, and, at an observation site close to, but equatorward of the cusp (as in the present examples), could produce field distortions of the observed sense. Other ideas may also be invoked, and will have to be tested in a systematic study of all the relevant data.

Acknowledgements

The authors wish to thank E. Skopke and I. Papamastorakis for programming support and data management. The Max-Planck-Institut portions of this work were supported by the Bundesministerium für Forschung und Technologie under grants RV14-B6/74 and O1 OI O 27-2A/WF/WRK 275:4. Work at Dartmouth was supported by NASA under grant NSG 5348 and by the National Science Foundation, Atmospheric Science Division, under grant ATM-7920277. Los Alamos portions were done under the auspices of the US Department of Energy with NASA support under S-50864A. Work at UCLA was supported under NASA contract NAS-5-25772.

**References**

- Akasofu, S.-I., E.W. Hones, Jr., S.J. Bame, J.R. Asbridge, and A.T.Y. Lui, Magnetotail and boundary layer plasmas at a geocentric distance of  $\sim 18 R_E$ : Vela 5 and 6 observations, J. Geophys. Res., 78, 7257-7274, 1973.
- Aubry, M.F., C.T. Russell, and M.G. Kivelson, Inward motion of the magnetopause before a substorm, J. Geophys. Res., 75, 7018-7031, 1970.
- Bame, S.J., J.R. Asbridge, H.E. Felthouser, J.P. Glore, G. Paschmann, P. Hemmerich, K. Lehmann, and H. Rosenbauer, ISEE-1 and ISEE-2 fast plasma experiment and the ISEE-1 solar wind experiment, IEEE Transact. Geosci. Electron., GE-16, 216-220, 1978.
- Bame, S.J., J.R. Asbridge, J.T. Gosling, M. Halbig, G. Paschmann, N. Sckopke, and H. Rosenbauer, High temporal resolution observations of electron heating at the bow shock, Space Sci. Rev., 23, 75-92, 1979.
- Crooker, N.U., Explorer 33 entry layer observations, J. Geophys. Res., 82, 515-522, 1977.
- Eastman, T.E., E.W. Hones, Jr., S.J. Bame, and J.R. Asbridge, The magnetospheric boundary layer: Site of plasma, momentum and energy transfer from the magnetosheath into the magnetosphere, Geophys. Res. Lett., 3, 685-688, 1976.

Eastman, T.E., The plasma boundary layer and magnetopause layer of the Earth's magnetosphere. PhD thesis. University of California, Los Alamos Scientific Laboratory, preprint LA-7842-T, 1979.

Eastman, T.E., and E.W. Hones, Jr., Characteristics of the magnetospheric boundary layer and magnetopause layer as observed by IMP 6, J. Geophys. Res., 84, 2019-2028, 1979.

Fairfield, D.H., Average and unusual locations of the earth's magnetopause and bow shock, J. Geophys. Res., 76, 6700-6716, 1971.

Frank, L.A., K.L. Ackerson, R.J. DeCoster, and B.G. Burek, Three-dimensional plasma measurements within the earth's magnetosphere, Space Sci. Rev., 22, 739-763, 1978.

Haerendel, G., Microscopic plasma processes related to reconnection, J. Atmos. Terr. Phys., 40, 343-353, 1978.

Haerendel, G., and G. Paschmann, Entry of solar wind plasma into the magnetosphere, in: Physics of the Hot Plasma in the Magnetosphere (B. Hultquist and L. Stenflo, ed.s), pp. 23-43, New York (Plenum) 1975.

Haerendel, G., G. Paschmann, N. Sckopke, H. Rosenbauer, and P.C. Hedgecock, The frontside boundary layer of the magnetosphere and the problem of reconnection, J. Geophys. Res., 83, 3195-3216, 1978.

- Hones, E.W., Jr., J.R. Asbridge, S.J. Bame, M.D. Montgomery, S. Singer, and S.-I. Akasofu, Measurements of magnetotail plasma flow made with Vela 4B, J. Geophys. Res., 77, 5503-5522, 1972.
- Mead, G.D., and D.H. Fairfield, A quantitative magnetospheric model derived from spacecraft magnetometer data, J. Geophys. Res., 80, 523-534, 1975.
- Paschmann, G., G. Haerendel, N. Sckopke, H. Rosenbauer, and P.C. Hedgecock, Plasma and magnetic field characteristics of the distant polar cusp near local noon: The entry layer, J. Geophys. Res., 81, 2883-2899, 1976.
- Paschmann, G., N. Sckopke, G. Haerendel, J. Papamastorakis, S.J. Bame, J.R. Asbridge, J.T. Gosling, E.W. Hones, Jr., and E.R. Tech, ISEE plasma observations near the subsolar magnetopause, Space Sci. Rev., 22, 717-737, 1978.
- Paschmann, G., B.U.Ö. Sonnerup, I. Papamastorakis, N. Sckopke, G. Haerendel, S.J. Bame, J.R. Asbridge, J.T. Gosling, C.T. Russell, and R.C. Elphic, Plasma acceleration at the earth's magnetopause: Evidence for reconnection, Nature, 282, 243-246, 1979.
- Peterson, W.K., E.W. Hones, Jr., E.G. Shelley, R.D. Sharp, H. Balsiger, S.J. Bame, and G. Paschmann, Measurements of  $O^+$  and  $He^{++}$  in the low latitude boundary layer from ISEE-1, EOS, Transact. AGU, 60, 929, 1979 (abstract).

Ogilvie, K.W., T. von Rosenvinge, and A.C. Durney, International sun-earth explorer: A three-spacecraft program, Science, 198, 131-138, 1977.

Rosenbauer, H., H. Grünwaldt, M.D. Montgomery, G. Paschmann, and N. Sckopke, Heos 2 plasma observations in the distant polar magnetosphere: The plasma mantle, J. Geophys. Res., 80, 2723-2737, 1975.

Russell, C.T., The ISEE 1 and 2 fluxgate magnetometers, IEEE Transact. Geosci. Electron., GE-16, 239-242, 1978.

Russell, C.T., and R.C. Elphic, Initial ISEE magnetometer results: Magnetopause observations, Space Sci. Rev., 22, 681-715, 1978.

Shelley, E.G., W.K. Peterson, G. Haerendel, G. Paschmann, and H. Balsiger, On the origin of the magnetospheric boundary layer plasma, EOS, Transact. AGU, 59, 1163, 1978 (abstract).

Sonnerup, B.U.Ö., Magnetopause and boundary layer, in: Physics of Solar Planetary Environments (D.J. Williams, ed.), pp. 541-557, Washington, D.C. (AGU) 1976.

Sonnerup, B.U.Ö., Theory of the low-latitude boundary layer, J. Geophys. Res., 85, 2017-2026, 1980.

Figure 1

Figure 1: Plasma and magnetic-field data from an ISEE out-bound pass through the outer magnetosphere, low-latitude boundary layer, and magnetosheath; near 0800 hours local time and  $40^\circ$  northern GSM latitude. The plasma parameters are, from top to bottom: proton ( $N_p$ ) and electron ( $N_e$ ) densities in units of  $\text{cm}^{-3}$  as solid and dotted curves, temperature  $T_p$  and  $T_e$  in Kelvin, and proton bulk speed ( $v_p$ ) in  $\text{km s}^{-1}$ . The data are from the LASL/MPE two-dimensional instrument with points obtained every 3 s, and displayed every 24 s. Magnetic-field data (lower three panels) are 64-s averages obtained from the UCLA magnetometer, and are given as GSM azimuth ( $\phi_B$ ) and elevation ( $\lambda_B$ ) angles and field magnitude,  $B$ , in gammas. Density levels 1-4 indicate characteristic values for the outer magnetosphere, boundary layer halo, boundary layer proper, and magnetosheath, respectively (cf. Figure 7 for a physical model).

Figure 2: Proton and electron partial densities, i.e. contributions from certain energy bands to the total densities shown in Figure 1. Units are  $\text{cm}^{-3}$ , and the curves are displaced by two decades each. The vertical line near 0550 UT marks the magnetopause crossing.

Figure 3: Details of the boundary layer observations. The upper three panels show the proton density and temperature, and the proton pressure ( $P_p$ , lower curve) as well as the

total pressure,  $P_T = P_p + B^2/8\pi$ , both in units of  $10^{-8}$  dynes  $\text{cm}^{-2}$ . The central three panels display the proton flow behaviour. The  $v_p$  panel shows both the bulk speeds derived from the 2D and 3D instruments. Note the good agreement between the two curves everywhere except near steep gradients (where the 3D sampling time is too long) and in the magnetosheath, after 0550 UT (where the temperature is too low for the 3D instrument to resolve the distributions adequately).  $\alpha_p$  measures the flow azimuth in the local tangential plane of the magnetopause, with  $\alpha_p = 0$  indicating a perfectly symmetric tailward flow (away from the stagnation point).  $c_p$  measures the flow elevation from this plane, with  $c_p > 0$  indicating an outward directed component. (NOR system, cf. the label on the left of these panels). Note that  $\alpha_p$  and  $c_p$  are not displayed for  $N_p \cdot v_p < 10^7 \text{ cm}^{-2} \text{ s}^{-1}$ . The lower three panels show the magnetic field as magnitude (B), and azimuth ( $\alpha'_B$ ) and elevation ( $c'_B$ ). These angles are similarly defined as the plasma flow angles except that  $\alpha'_B = 0$  points towards GSM north (LMN system of Russell and Elphic). NOR and LMN are based on the Fairfield model magnetopause normal for the spacecraft position at 0550 UT. In the present case,  $\alpha(\text{NOR}) = \alpha'(\text{LMN}) - 60^\circ$ , cf. the NOR scale on the right-hand side of the  $\alpha'_B$  panel. Vertical lines mark the more prominent leading edges of boundary layer density variations and the magnetopause crossing.

Figure 4: Hodograms of the magnetic field vector (in units of nT) for the ISEE-1 magnetopause crossing, shown in the principal axes coordinate system obtained from a minimum variance

analysis. The  $i$  and  $k$  axes are the directions of maximum and minimum variance of the field, respectively; all three are rather closely aligned with their respective counterparts of the LFN system employed for the previous and subsequent figure. The  $(i, j)$  plane on the left is tangential to the magnetopause, and the  $(i, k)$  plane corresponds to a meridional cut with  $k$  being the outward directed normal to the boundary.

Figure 5: Proton densities and field azimuth angles in the tangential plane ( $\alpha'_B = \tan^{-1}(B_M/B_L)$ ) in the vicinity of the magnetopause crossings as seen by ISEE-1 (solid curves) and ISEE-2 (dots). Data are displayed every 1.5 s. ISEE-1 was 510 km further outward than ISEE-2, with the separation vector being almost parallel to the model (and minimum variance) normal.

Figure 6: ISEE-1 and -2 proton densities (solid and dotted curves, respectively) during the earlier boundary layer encounters, showing the time delays between certain features as seen by the two spacecraft. Letters a-l mark those interfaces for which normal vectors are displayed in Figure 8. Note that, because of an ISEE-2 data gap, panels 2 and 3 are not contiguous.

Figure 7: Three models to explain the observations: (A) a uniform boundary layer attached to a smooth magnetopause, both oscillating together about their normal position with speed  $v_n$ ; (B) a uniform attached boundary layer disturbed, as the magnetopause, by surface waves; and (C) a boundary layer of non-uniform thickness attached to a smooth magnetopause. The observations

favour model C (although elements of A and B are present; cf. the text). In this model, regions 1-4 denote the outer magnetosphere, halo, boundary layer proper, and magnetosheath, respectively (cf. Figure 1 for the corresponding density (and temperature) levels). The open arrows denote, as in models A and B, plasma flow in the spacecraft frame of reference. The flow vortex (dashed curve) and the satellite path, are shown for a moving system in which the boundary layer structure is (approximately) at rest.  $z_N$  is the model magnetopause normal, and  $n$  is the boundary layer normal pointing into region 2 (cf. Figure 3).

Figure 8: Boundary layer normals at the halo interface derived from density gradients a-1 in Figure 6 and from simultaneous field rotations if present (cf. Figure 3).  $\Delta t = t_2 - t_1$  are the time delays (in seconds) with which the respective gradients were observed by the two spacecraft. Each individual diagram shows projections of the boundary layer normals onto the  $(x_N, z_N)$  plane of the NOR system in which  $z_N$  is the model magnetopause normal, and  $x_N$  is the direction of the symmetric magnetosheath flow. The sectors with radii of short and intermediate lengths indicate a range of directions derived from the plasma and field data on the low- and high-density side of the discontinuity, respectively ( $\underline{U} \times \underline{B}$  method, cf. the text). Symbols were not drawn when (data were missing or) the plasma bulk speed was low and hence when statistical errors were large. The long arrows are based on the  $\underline{B}_2 \times \underline{B}_3$  method described in the text. To avoid cluttering the figure, only the average

direction was drawn, with spreads in angle being typically less than  $\pm 5^\circ$ . Larger variations ( $\pm 10^\circ$ ) occurred when also the two  $\underline{U} \times \underline{B}$  normals differed significantly from each other. Arrows were not drawn when the field rotated by less than  $15^\circ$ .

Figure 9: Plasma and field data for another ISEE pass showing basically the same features as Figure 1.

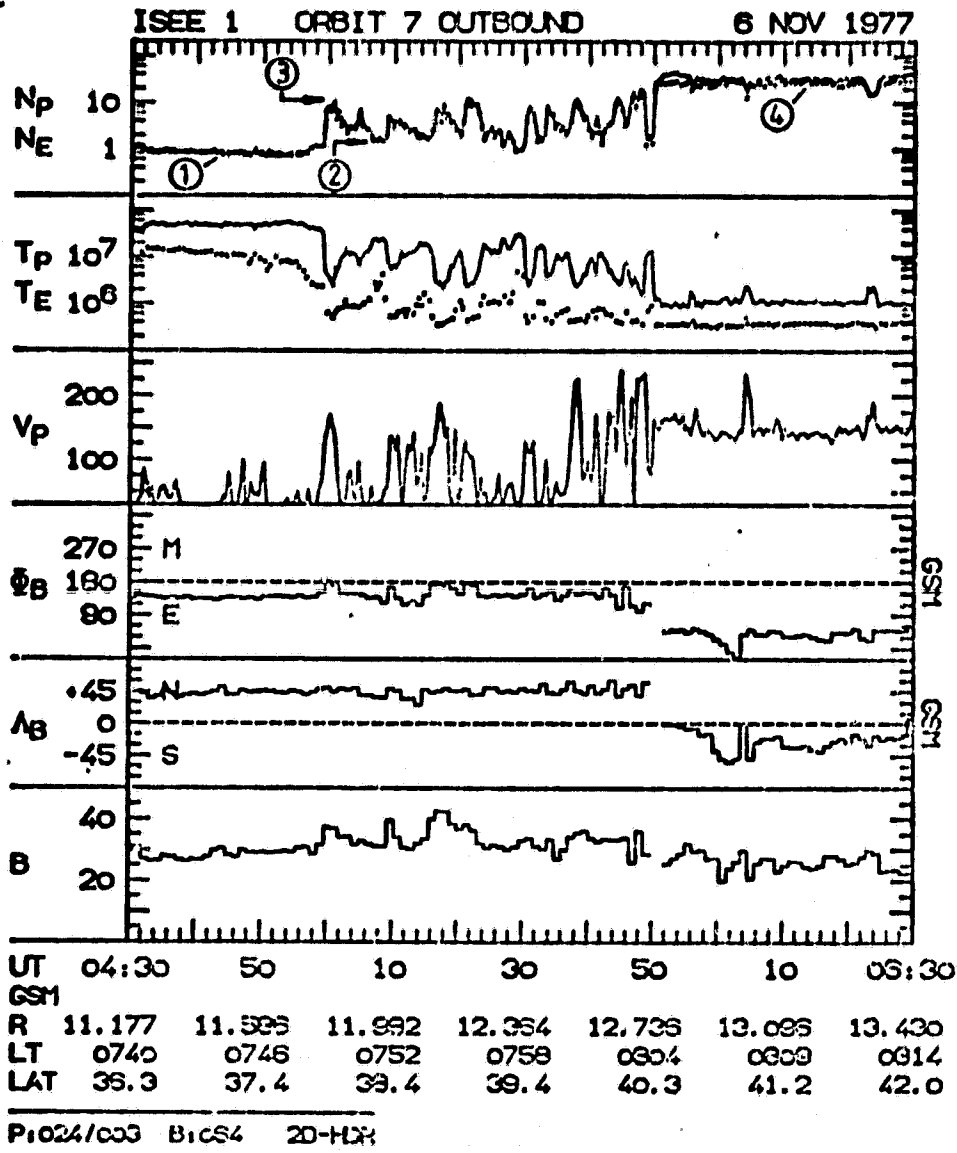


Figure 1

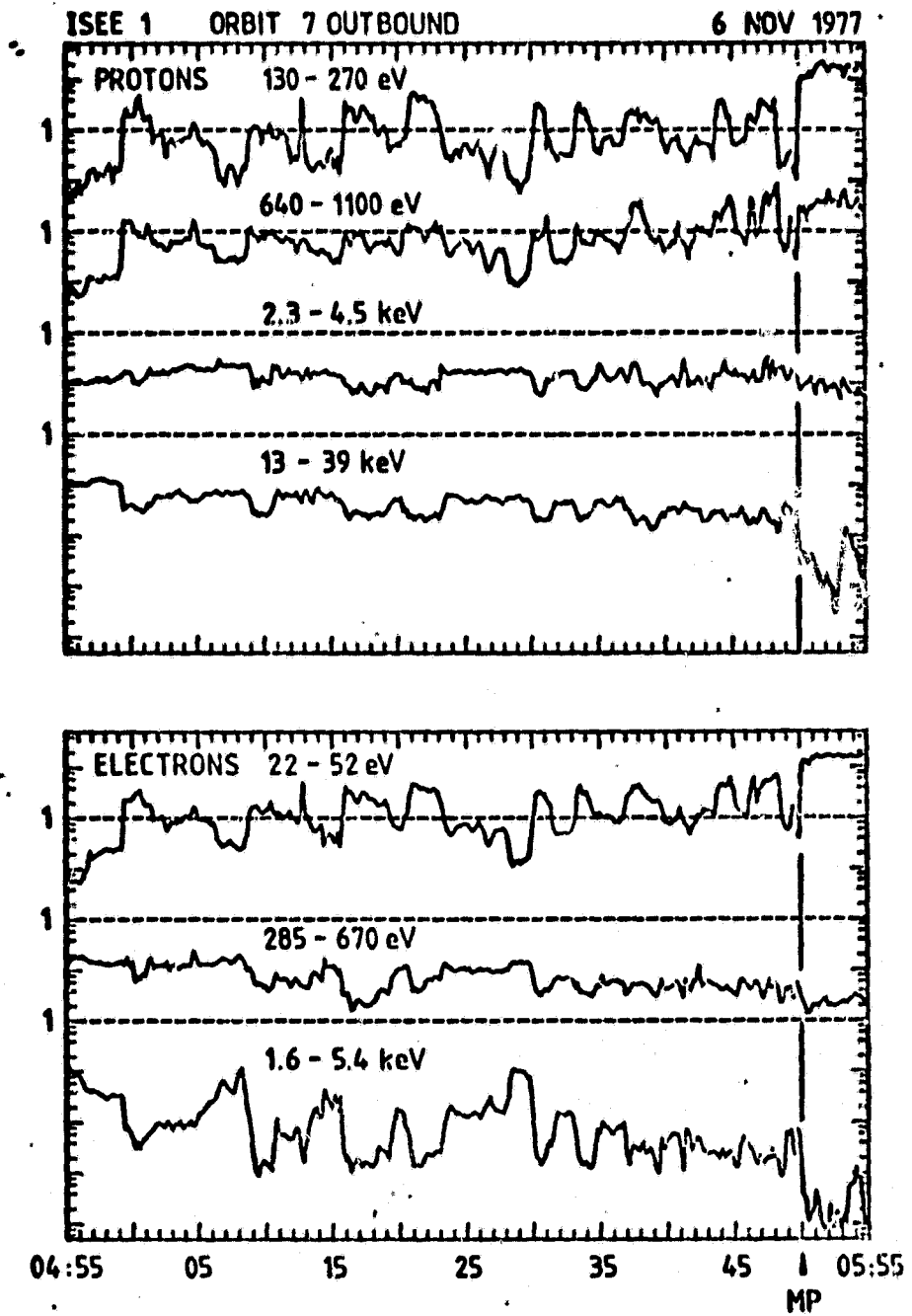


Figure 2

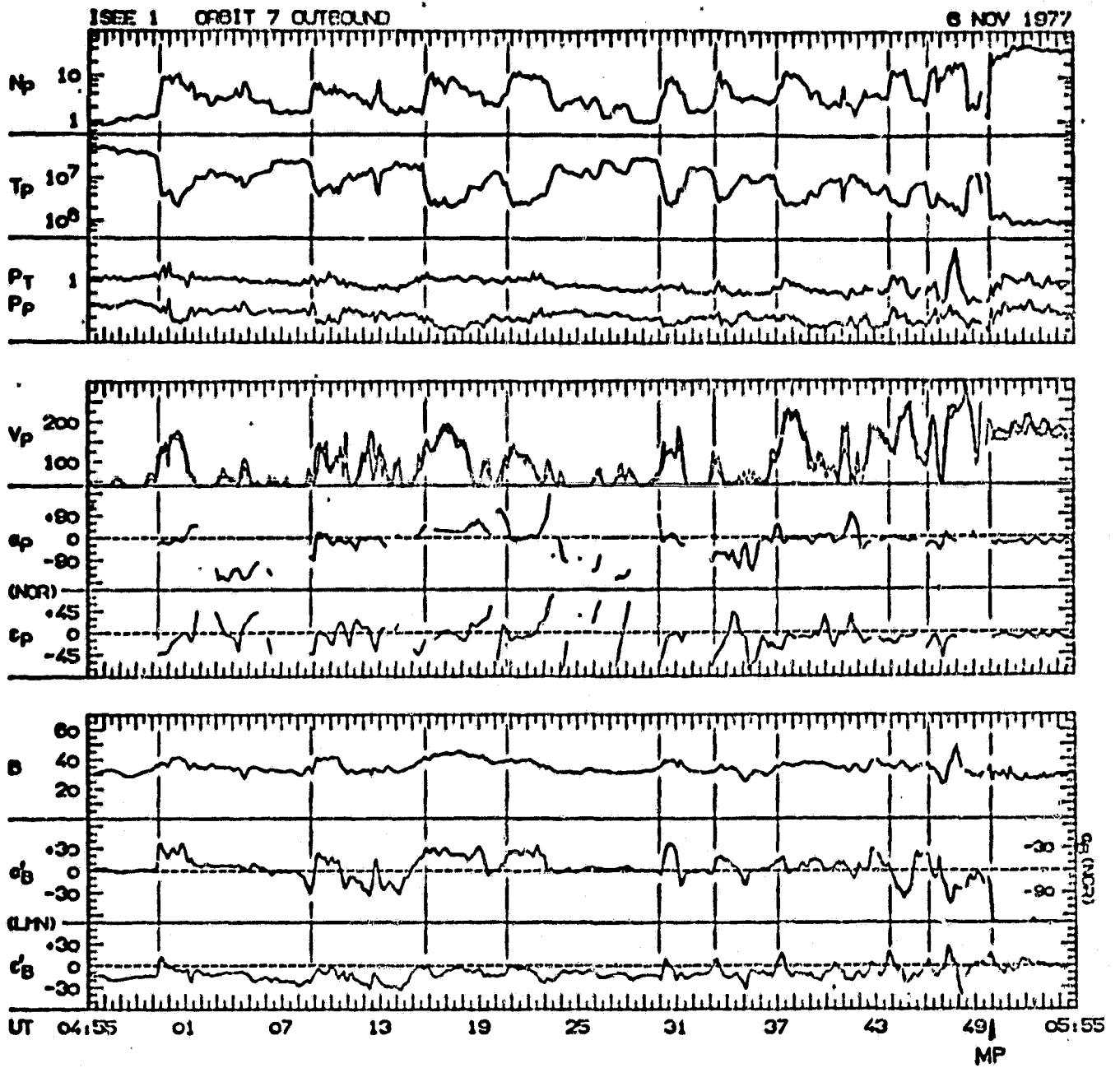


Figure 3

ISEE. 2 6 NOV 1977  
05:50:09 - 05:50:35

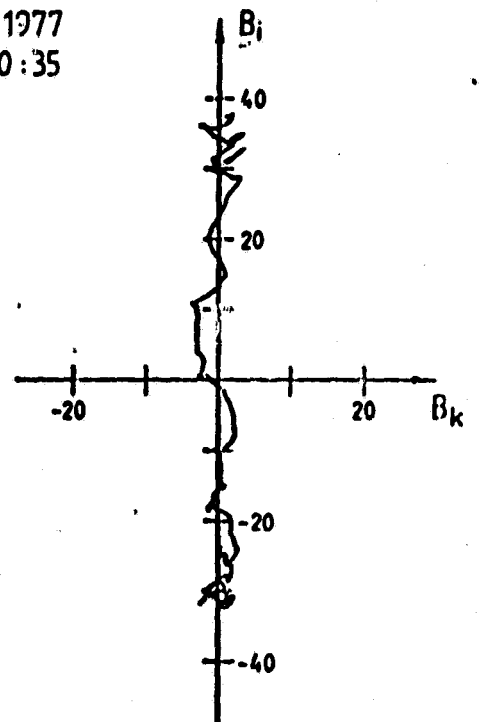
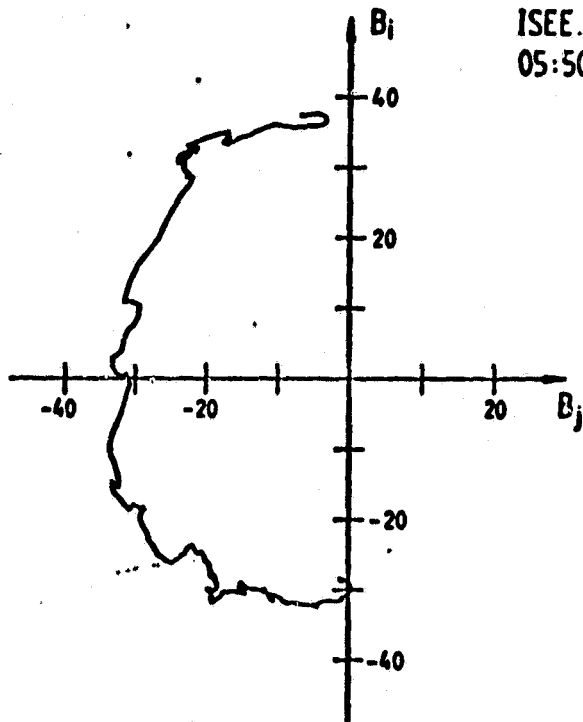


Figure 4

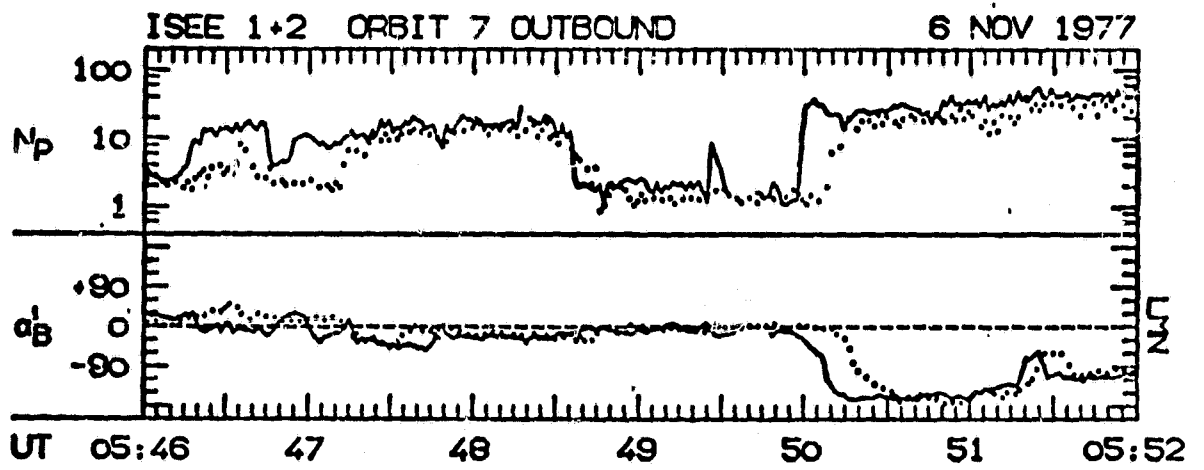


Figure 5

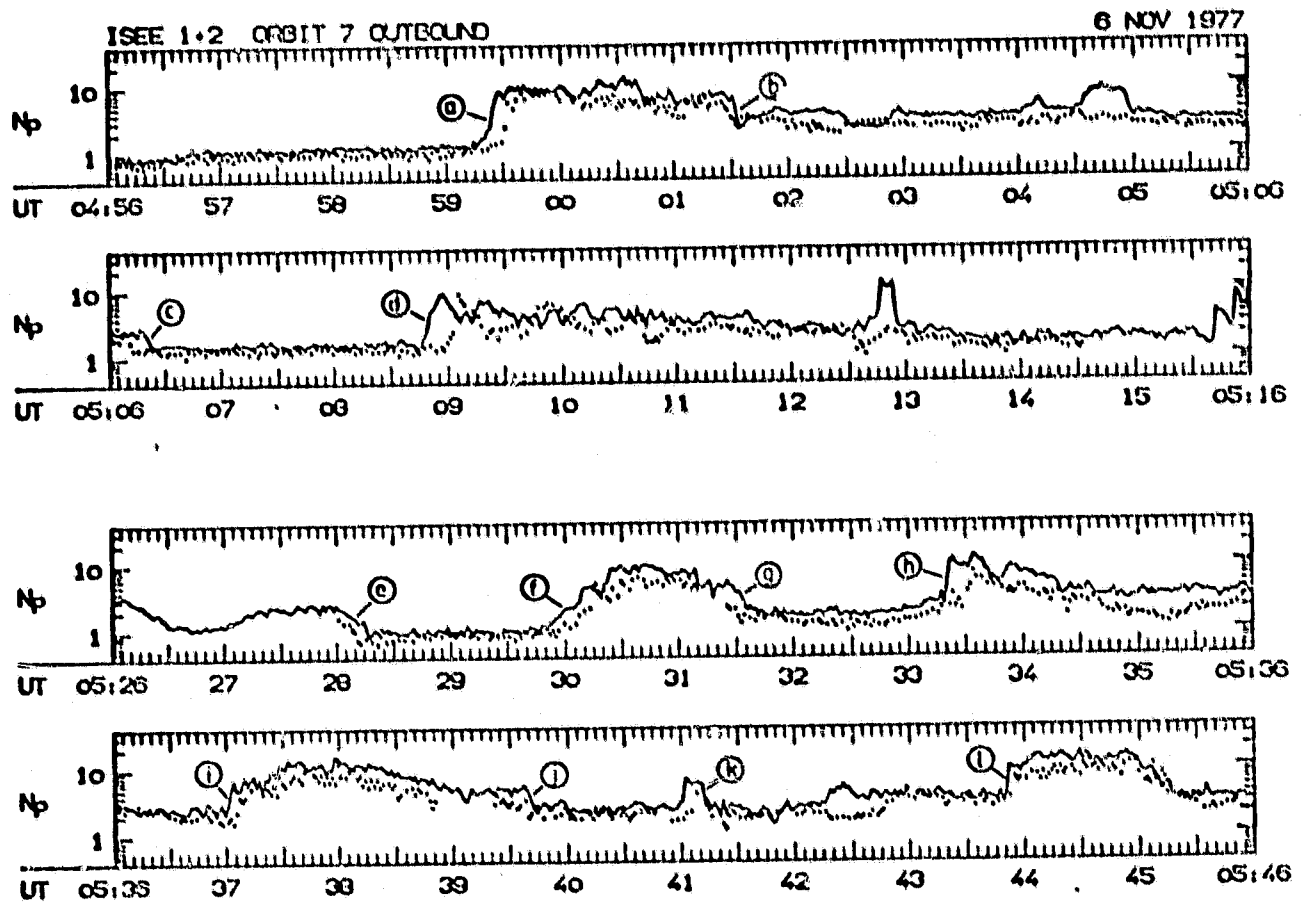


Figure 6

ISEE 1+2 ORBIT 7 OUTBOUND

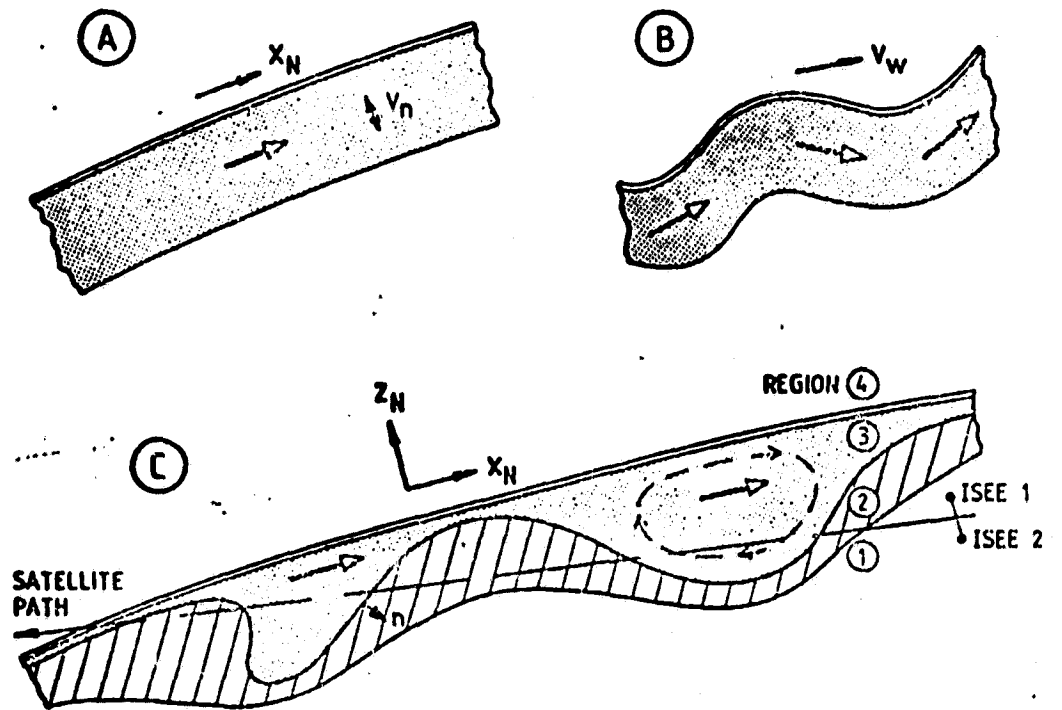
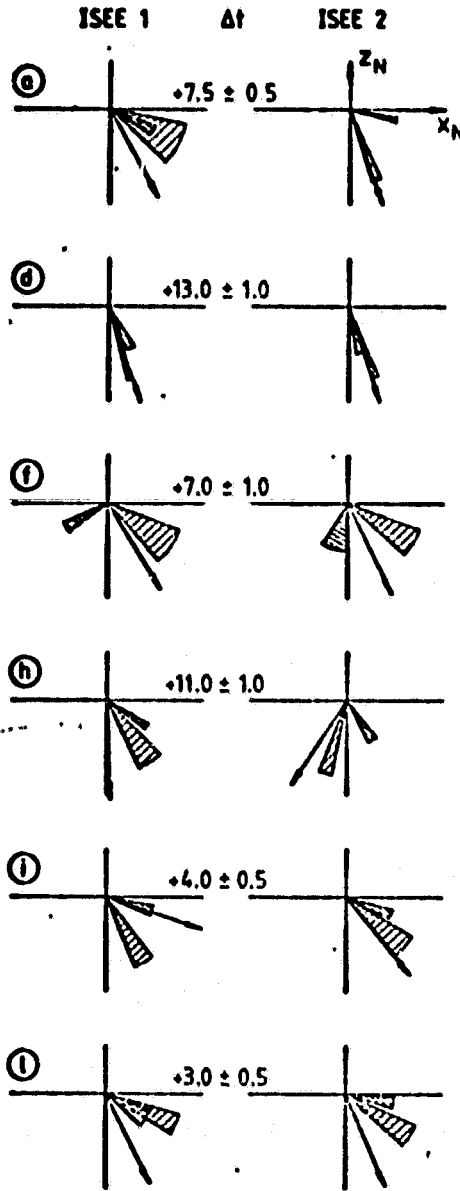


Figure 7

### Leading Edges



### Trailing Edges

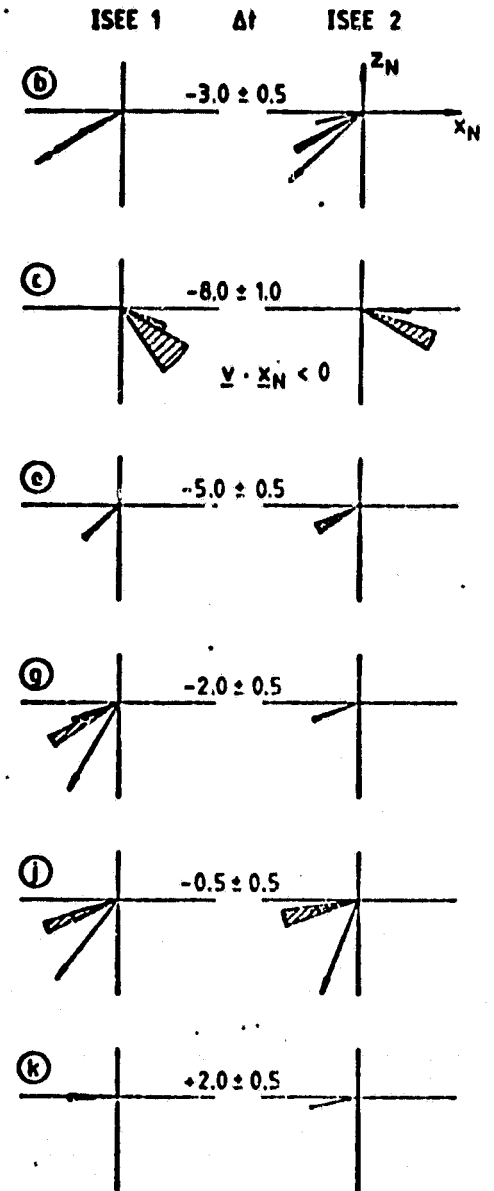


Figure 8

ISEE 1 ORBIT 12 OUTBOUND 18 NOV 1977

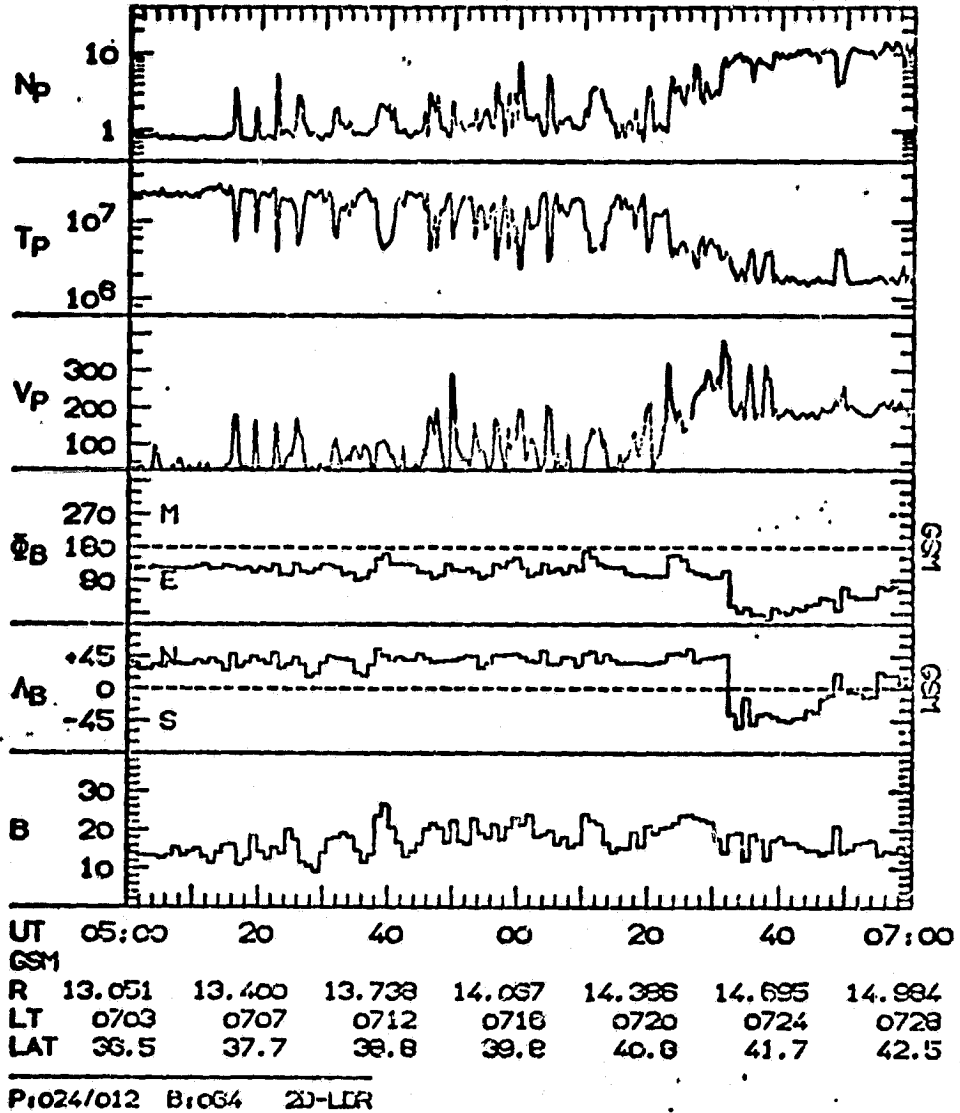


Figure 9

ORIGINAL PAGE IS  
OF POOR QUALITY